Geo-information Science and Remote Sensing

Thesis Report GIRS-2024-14

Reconstruction of NDVI time series based on SAR data using a deep learning method

Yongjin Wang

May 10, 2024

WAGENINGEN
UNIVERSITY & RESEARCH

Reconstruction of NDVI time series based on SAR data using a deep learning method

Yongjin Wang

Registration number: 11 98 718

Supervisors:

dr.ir. JGPW (Jan) Clevers
ir. GJ (Gerbert) Roerink
dr. MJ (Maciej) Soja

A thesis submitted in partial fulfilment of the degree of Master of Science
at Wageningen University and Research,
The Netherlands.

May 10, 2024
Wageningen, The Netherlands

Thesis code number: GRS-80436
Thesis Report: GIRS-2024-14
Wageningen University and Research
Laboratory of Geo-Information Science and Remote Sensing

Foreword

This thesis uses the U-net model to reconstruct NDVI time series based on SAR data, which can be divided into three main parts. The first part is model training, where a total of nine models are trained depending on the input data for regressing NDVI images. The second part involves NDVI prediction and time series construction. In this section, the nine trained models are used for predicting NDVI images, and subsequently, NDVI time series for different crops are established based on these predictions. The final part is evaluating the quality of the reconstructed NDVI time series, focusing primarily on two aspects. Firstly, at the temporal level, the quality of the average NDVI time series among all parcels is evaluated. Secondly, the reconstructed NDVI time series are used in the Cropmarkers algorithm developed by Wageningen Environmental Research to detect important time points in crop growth cycles, assessing the feasibility of the method used in this thesis in practical applications.

This research serves as the thesis for my Master's program in Geo-information Science at Wageningen University. Through this program, I gained a lot of knowledge in remote sensing and a strong internet in its applications in vegetation monitoring. The topic of this thesis applies deep learning techniques, combining optical and radar remote sensing for agricultural monitoring, which aligns well with my expertise and interests. I believe it can lay a solid foundation for my future career path.

Many people helped me with my thesis research and writing. First of all, I would like to thank my three supervisors, Jan Clevers, Gerbert Roerink and Maciej Soja, for supervising my thesis research and writing. Without their supervision and help, the thesis could not be completed smoothly. Specifically, I would like to thank Maciej Soja for his support in the implementation of the deep learning algorithm, and Adugna Mullissa (UCLA, formerly WUR) for his help in building the deep learning model. I would also like to thank Gerbert Roerink for his support in the application of the Cropmarkers algorithm and agricultural knowledge. I would also like to thank Jan Clevers for his responsible supervision of the progress of my thesis. In addition, I would like to thank Wageningen Environmental Research for providing the satellite data and Cropmarkers algorithm, and I would also like to thank Jappe Franke for his help in using the High-Performance Computer Anunna. Finally, I would like to thank Johannes Reiche for being the examiner to evaluate my thesis.

Yongjin Wang

10 May 2024, Wageningen

Abstract

The demand for agricultural production output is continuously increasing in the world of today, while climate change, disasters, and other issues threaten agricultural production and food security, placing higher demands on agricultural management. As a means of remote monitoring, remote sensing is widely used in agricultural monitoring due to its low cost and high efficiency, playing an important role in assisting agricultural management. The Normalized Difference Vegetation Index (NDVI) is a vegetation index calculated by the red and near-infrared bands of optical remote sensing images. It is closely related to crop growth and productivity characteristics, making it valuable in agricultural monitoring. However, optical remote sensing is highly sensitive to weather conditions and prone to cloud cover, leading to frequent data gaps in NDVI time series generated based on it. Since synthetic aperture radar (SAR) is independent of weather conditions, and SAR data has been proven to be related to NDVI, reconstructing the NDVI time series from SAR data is a potential solution. This study is based on the U-net model, which combines different Sentinel-1 SAR data and auxiliary data to train nine models. These models are used to reconstruct the NDVI time series of several crops in the Flevopolder region of the Netherlands in 2022, and are validated on the temporal scale. The modified Cropmarkers algorithm developed by Wageningen Environmental Research (WENR) is applied to the reconstructed NDVI time series to detect crop emergence, closure, transition, and harvest stages, thus validating the performance of the trained models in practical agricultural applications. The method used in this study achieves the best overall results for full canopy crops, with the corresponding R^2 values obtained for sugar beet, consumption potato, silage maize, and winter wheat being 0.92, 0.87, 0.67, and 0.82, respectively. Worse results were obtained for half canopy crops, with the R^2 values for tulip and onion being 0.56 and 0.67, respectively. This is probably due to the low proportion of half canopy crop parcels in the training dataset resulting in insufficient training. On grassland, the changes in NDVI data caused by mowing could not be predicted well. For full canopy crops, the reconstructed NDVI time series detected the four crop penological stages relatively well. The average deviation for crop emergence and closure ranged from 5 to 10 days, and for transition it was between 10 to 15 days. For harvest it varied from around ten to over twenty days depending on the crop type, while for half canopy crops the results were worse. Among the nine models, Model M51, which used multi-temporal backscatter data, crop identification maps, and year and week information as input layers, achieved the best overall performance, whereas adding 12-day interferometric coherence data did not improve model performance. Compared to the results of other literatures utilizing traditional machine learning algorithms, the method used in this study significantly improved the quality of the reconstructed NDVI time series, demonstrating the applicability of the U-net model over a larger spatial extent, and providing a solution for supplementing optical NDVI time series.

Keywords: NDVI, time series, reconstruction, Sentinel 1, Sentinel 2, SAR, U-net, deep learning

Contents

1. Introduction

1.1. Context and background

Agriculture is one of the pillars upon which humanity relies for survival and driving socio-economic development. With the continuous growth of population and income, there is an increasing demand globally for higher agricultural output (Johnson et al., 2014). However, factors such as climate change and disasters continuously challenge agricultural production and food security. Close monitoring of crop growth can assist in field management, thereby achieving more efficient agricultural production. Remote sensing is a technology that utilizes platforms such as aircraft or satellites to acquire ground information. Its principle is capturing electromagnetic waves reflected or emitted from the Earth surface using sensors, and then converting this information into visualized images or data using digital image processing techniques. In agricultural monitoring, remote sensing has advantages such as wide monitoring coverage, high observation frequency, and low costs for large-scale applications. It has become an efficient and reliable method widely applied in crop monitoring.

Vegetation indices based on optical remote sensing are important tools for achieving this purpose. Over the past few decades, many vegetation indices have been proposed, among which the Normalized Difference Vegetation Index (NDVI) is the most widely used, which can be calculated by the near-infrared (NIR) and red (R) bands (Eq. (1)) from optical remote sensing images.

$$NDVI = (NIR - R)/(NIR + R) \quad (1)$$

NDVI provides an intuitive reflection of vegetation greenness and is also associated with plant structural characteristics (Gamon et al., 1995; Turner et al., 1999) and productivity features (Gamon et al., 1995). Periodic recording of NDVI within a specific area results in an NDVI time series. NDVI time series reflect the dynamic changes of vegetation over time. In the field of agriculture, time series are commonly used for detecting crop phenological stages, monitoring agricultural activities, estimating crop yields, and more.

However, optical remote sensing is highly sensitive to weather conditions, particularly clouds and precipitation. Under cloudy conditions, optical sensors can be obstructed by cloud cover, leading to the inability to conduct normal observations. This can affect the regular acquisition of NDVI, and result in data loss, and exacerbating the complexity and challenges of remote sensing monitoring, especially in regions with high vegetation dynamics.

Since the first Landsat missions, the temporal, spatial, and spectral resolution of optical remote sensing imagery has continuously improved. With the launch of the Sentinel-2A and Sentinel-2B satellites as part of the Copernicus program in June 2015 and March 2017, respectively, this problem has been partially alleviated thanks to their low revisit period of 5 days (Drusch et al., 2012). However, more effective solutions are still needed.

Synthetic Aperture Radar (SAR) is an active remote sensing system capable of emitting radio- or microwave-frequency electromagnetic waves, enabling it to penetrate through clouds, haze, sand, and dust, etc. (Mirzaee et al., 2014). Moreover, research has demonstrated the relation between radar backscatter and NDVI during crop growth processes (Fieuzal et al., 2013). These characteristics make it interesting to predict NDVI data using SAR data and thereby reconstruct NDVI time series. The availability of SAR data has greatly increased on a global scale with the advent of the Sentinel-1 mission. Compared to previous SAR missions like ERS-1/2 SAR and ENVISAT ASAR, the Sentinel-1 constellation of two satellites provides a repeat cycle of 6 days and conflict-free operations, along with greater coverage (Torres et al., 2012). This allows SAR data to be similar in temporal resolution to optical data and to have a spatial resolution comparable to or slightly coarser than that of optical data, ensuring the reliability of NDVI time series reconstruction based on SAR data (Moreira et al., 2013).

1.2. Previous work

Methods for reconstructing and repairing NDVI time series can generally be divided into two categories based on the source of data. The first category relies on optical data itself. The other

category is based on radar data, regressing optical data based on the relationship between the two to reconstruct or repair optical time series.

1.2.1. Time series reconstruction based on optical data

The first category of reconstruction methods relies on the spatiotemporal information from optical data. In the early stages, this approach mainly relied on the temporal information derived from individual pixel values (Li et al., 2021). It involved methods such as function-based curve fitting, sliding windows filtering methods, and frequency domain approaches. These methods performed poorly with large temporal gaps and were sensitive to data variations. They also became ineffective when dealing with many anomalies in the time series, such as natural disasters and pest infestations. To address these issues, Xu et al. (2015) attempted to use the spatial similarity principle to reconstruct NDVI based on neighbouring pixel elements. However, existing cloud removal algorithms were not perfect, as they couldn't completely detect cloud shadows and fog. Cao et al. (2018) tried to incorporate spatial domain information to assist temporal filtering, but the spatiotemporal reference information was still not fully utilized.

To address the aforementioned issues, some studies have tried to fuse data from different optical sensors (Gao et al., 2017; Griffiths et al., 2020). However, these multi-sensor approaches require calibration to harmonize different spatial and spectral resolutions. Additionally, supplementary optical data used for this purpose may also be affected by cloud cover, thereby not guaranteeing the provision of a substantial amount of reliable supplementary observations (Garioud et al., 2021)

1.2.2. Time series reconstruction based on Radar data

Since SAR observations are not affected by cloud cover, an increasing number of studies in recent years have utilized SAR data to reconstruct time series of optical vegetation indices. These studies can generally be classified into three categories: classical machine learning algorithms (Random Forest (RF), Support Vector Machine (SVM)), Gaussian Process (GP) technique, and deep learning algorithms.

In many studies, classical machine learning algorithms have been applied. Mohite et al. (2020) conducted regression analyses using NDVI as the independent variable, polarimetric SAR backscatter, and some auxiliary information as dependent variables, employing RF and SVM algorithms to estimate NDVI time series for several crops. Wang et al. (2019) applied SVM and RF algorithms on Sentinel-1, Sentinel-2, and Landsat-8 data, estimating Leaf Area Index (LAI). Although traditional machine learning algorithms have achieved satisfactory results in these studies, the agricultural datasets used for validation are generally small-scale, and the variety of crops included is very limited, thus not guaranteeing the effectiveness of these techniques when applied to large-scale areas.

The second category of methods involves the use of the Gaussian Process (GP) technique. GP is a machine learning technique primarily applied to regression and probabilistic classification problems in supervised learning. Pipia et al. (2019) trained a Multi-Output Gaussian Process (MOGP) model using Sentinel-1 Radar Vegetation Index (RVI) and Sentinel-2 Leaf Area Index (LAI) time series to fill in missing values in the LAI time series. Besides time series reconstruction, GP has also been applied in other regression tasks for vegetation monitoring. Mercier et al. (2020) utilized Gaussian process regression combined with Sentinel-1 and Sentinel-2 time series to extract biophysical parameters from various crop parcels. While the performance of GP in such regression tasks has been confirmed, GP tuning is complex, sensitive to kernel selection, and requires extensive computational resources and long training time, which makes its scalability questionable as well.

The third category of methods involves the use of deep learning techniques for time series reconstruction. Deep learning serves as a data-driven model capable of accurately extracting and representing information from large-scale satellite images. The continuous advancement of computer performance and the increased availability of large datasets greatly support its development and application. In recent years, the powerful feature extraction capabilities of deep learning algorithms have attracted significant attention (Li et al., 2022). Scarpa et al. (2018) conducted experiments in a small agricultural area in Burkina Faso using a small convolutional

neural network (CNN) to predict NDVI from Sentinel data for the period from May to November, achieving good prediction results when both optical and SAR data were used as inputs. In this study, satellite images before or after the target date were also used for neural network training to capture temporal information. Roßberg and Schmitt (2023) used a modified U-net model with Sentinel data to predict NDVI imagery for different vegetation cover areas around the globe. SAR backscatter and NDVI images from the same day, along with some auxiliary images, were used for training, resulting in relatively close results across all vegetation cover types. Currently, image-based deep learning methods still face challenges related to small training datasets and questionable scalability when applied to specific fields like agriculture. Moreover, these methods often focus primarily on spatial validation, with less attention on temporal scale validation and the performance of reconstructed time series in practical applications. Additionally, the input data used for model training still needs further exploration to achieve better NDVI prediction results. Apart from these methods, another approach involves regression based on SAR time series. Zhao et al. (2020) proposed a regression method based on the Multi-CNN-Sequence to Sequence (MCNN-Seq) model. It first uses a one-dimensional convolutional neural network (CNN) to extract feature information from the time series of VH and VV polarizations of SAR data. Subsequently, these features are input into a long short-term memory (LSTM) model to capture the relationship between SAR data and target NDVI time series. Compared to the previous category of methods, this approach pays more attention to extracting information at the temporal scale. Although this method has shown promising results, it requires complete time series for learning, thus lacking flexibility and failing to meet the real-time application needs of fields such as agricultural monitoring.

1.3. Research objectives and questions

Deep learning provides a promising method for predicting NDVI from SAR data, and there is still considerable room for improvement in the use and training of deep learning models. Furthermore, validation of model predictions at the temporal scale and their performance in specific applications require further exploration.

The focus of this study is on constructing NDVI time series for agricultural crop applications. Radar data will be studied for filling gaps in optical time series. This study concentrates on the agricultural domain, employing deep learning models with U-net architecture to reconstruct NDVI time series for various crops. The applicability of the models for different crops in the study area is investigated, and the impact of different types of input data on model performance is evaluated. Additionally, to validate the performance of the predicted NDVI time series in practical applications, the Cropmarkers algorithm developed by Wageningen Environmental Research (WENR) is adopted to assess the performance of the reconstructed time series in detecting crop phenological stages and agricultural activities. The research questions of this study are as follows:

(1) How applicable is the NDVI time series reconstructed by this method to different types of crops?

> (a) How does the reconstructed time series compare to the reference NDVI time series (from optical data) in terms of overall differences and correlation?
>
> (b) How does the reconstructed time series perform in detecting crop phenological stages and agricultural activities?

(2) Can combining multiple types of data for training improve the U-net model performance compared to using solely multi-temporal SAR backscatter data?

> (a) How does the addition of 12-day coherence data affect the model performance?
>
> (b) Can the addition of the crop identification map and year and week information improve the model performance?

2. Data and methods

Figure 1 illustrates the research process of this study. The research process is divided into three parts. The first part focuses on model optimization and training for different combinations of input data. In the second part, based on the different models trained in the first part, NDVI images are predicted, followed by plot-level reconstruction of NDVI time series. The third part concentrates on quality assessment of the NDVI time series reconstructed using different models. Firstly, the quality of the average time series for each crop is assessed to estimate overall performance. Subsequently, the adjusted Cropmarkers algorithm is employed to predict key time points during the crop growth cycle, aiming to evaluate the performance of the reconstructed time series in practical agricultural applications.

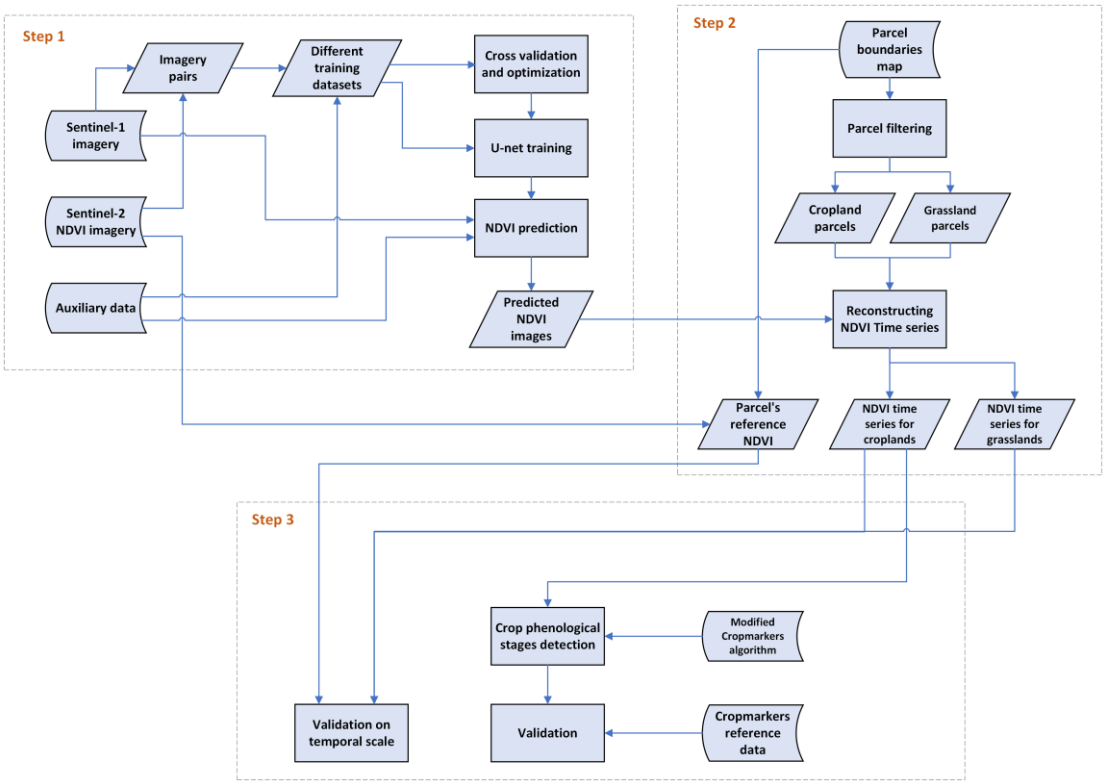

Figure 1. Overview of the research process.

2.1. Study area

The research area of this study is the Flevopolder region in the central part of the Netherlands, situated at the center of the Flevoland province. Flevopolder is reclaimed land characterized by sandy and loamy soil. Initially submerged by the Markermeer and IJsselmeer lakes, extensive drainage and land reclamation efforts transformed it into farmland. The location and land cover of this area are depicted in Fig 2. Since the majority of the land cover type in the region is agricultural fields with a wide variety of crops, it provides favourable conditions for this study.

Figure 2. Flevopolder study area

2.2. Data

In this study, Sentinel-1 and Sentinel-2 NDVI images based on date matching constitute the main part of the model training data, and the remaining auxiliary data include crop identification maps and year and week information. Parcel boundary maps are employed to assist in generating parcel-level NDVI time series for each crop. Cropmarkers reference data is used to validate the results obtained by the adjusted Cropmarkers algorithm on the reconstructed NDVI time series.

2.2.1. Satellite data

Sentinel-1 data

Sentinel-1 is a mission initiated by the European Space Agency (ESA) in 2014, aimed at providing all-weather, high-resolution Synthetic Aperture Radar (SAR) surface monitoring data. The Sentinel-1 constellation includes two satellites, Sentinel-1A and Sentinel-1B (not operational since December 2021), positioned in orbits at an altitude of 698 kilometers. They have a phase difference of 180 degrees and revisit the same area every 12 days. Sentinel-1 provides SAR observation data in the C-band (5.5 cm wavelength) with dual polarization, with a single-look spatial resolution in the interferometric wide swath mode of about 4 x 23 meters in the ground range and azimuth directions, respectively. The Sentinel-1 data utilized in this study, including backscatter images, coherence images, and incidence angle maps, are provided by WENR.

Backscatter refers to the strength of the radar signal returned to the radar receiver after interacting with the Earth surface. Its magnitude depends on the structure and moisture of the Earth surface, as well as the wavelength, polarisation and incidence angle of the SAR system. Thus backscatter images can be used to identify surface features, land cover types, and monitor surface changes. For backscatter images, WENR obtained Single Look Complex (SLC) data and processed them using ESA SNAP and GDAL. The processing steps included applying precise orbit files, co-registration, calibration, multi-looking using a 5 x 1 window, terrain correction, and linear to decibel (dB) conversion. Finally, dual-polarization (VH, VV) backscatter images are obtained.

Coherence images were generated from two complex-valued SAR images acquired 12 days apart over the same area. They reflect the temporal stability of the Earth surface, playing an important role in monitoring surface changes. The coherence ranges from 0 to 1, where a coherence of 1 indicates complete similarity between the two images, while a coherence of 0 indicates complete dissimilarity. The processing steps included applying precise orbit files, co-registration, calibration, coherence estimation using a 19 x 4 window, and terrain correction. Finally, all strip areas from the same overpass were merged into a single coherence image with a spatial resolution of roughly 60 meters.

As the training data of the model included data from two adjacent orbits from the descending pass, this study also used the local incidence angle map. It contained information about the angle at which radar waves interact with the Earth surface at each pixel location in SAR images. The local incidence angle map was derived by WENR based on the DEM normals, taking into account the local slope calculated from the reference DEM.

Sentinel-2 data

The purpose of the Sentinel-2 mission is to provide global coverage of high-resolution multispectral imagery with a high revisit frequency, enhancing the continuity of multispectral imagery provided by the French SPOT satellite series and providing data for further observation products (Spoto et al., 2012). The Sentinel-2 constellation comprises two satellites, Sentinel-2A and Sentinel-2B, launched as part of the Copernicus program in June 2015 and March 2017, respectively, to collect spectral reflectance data of the Earth surface. With a revisit period of ten days at the equator for each satellite, the Sentinel-2 constellation can observe the Earth every five days (Drusch et al., 2012).

This study utilized NDVI images provided by WENR. After atmospheric correction of Sentinel-2 data, WENR calculated NDVI based on the near-infrared and visible red bands and obtained NDVI images with a resolution of 10 meters. In cases where cloud cover is present in the images, regions with low cloud cover ratios are filtered out. If there is too much cloud coverage, experts determine whether to process the images. Generally, images with cloud cover exceeding approximately 95% are not processed.

2.2.2. Parcel boundary map and crop identification map

The Parcel Boundaries map contains information on parcel boundaries and crop type in the Netherlands. It is based on the Basis Registratie Percelen (BRP), which is the Dutch equivalent of the EU mandatory Land Parcel Information System (LPIS).

Due to the varying proportions of pixels representing different crops in the training data, the model may perform poorly on crops with fewer training data. To mitigate this effect and help the model in better identifying each crop, this study created a crop identification map based on the "GEWASCODE" field in the Parcel boundary map (Figure 3). Parcels with the same crop type are uniquely identified by a specific value.

Figure 3. Crop Identification map of Flevoland for 2022 as used in this study

2.2.3. Year and week information

Since the training dataset of this study includes Sentinel data from multiple years, some factors such as seasonality and weather conditions may lead to overall differences between data from different years and dates. To account for this during model training, this study added year and week information in each set of training data, in the form of dummy value images.

2.2.4. Cropmarkers reference data

The Cropmarkers reference data contains information about key growth stages and harvest times of crops within each parcel in the Netherlands throughout the year. This data is obtained through the application of the Cropmarkers algorithm (Groenmonitor, n.d.) on NDVI time series and radar coherence time series. WENR hosts a website (https://www.groenmonitor.nl/) containing NDVI time series for each crop parcel within the Netherlands. WENR applies the Cropmarkers algorithm to these time series as well as to the coherence time series generated from Sentinel-1A and 1B, thereby estimating the dates of several key points in the crop growth cycle. In this study, this reference data is utilized to validate the results obtained from the adjusted Cropmarkers algorithm applied to the reconstructed NDVI time series.

2.3. Methods

2.3.1. Model training

2.3.1.1 Model structure

This study uses a model with a U-net architecture (Figure 4). The U-net model is a well-established model used for pixel-wise regression and semantic segmentation, widely applied in the field of remote sensing (Fan et al., 2022). The U-net model features an encoder-decoder structure. The encoder is responsible for extracting and compressing valuable features from the input data. It consists of multiple sets of 3x3 convolutional layers, followed by Rectified Linear Unit (ReLU) activation functions applied element-wise to each feature. Between each set of convolutional layers, 2x2 max-pooling operations are employed to downsample the features, reducing the spatial resolution of the data while doubling the number of channels. The decoder, on the other hand, generates the final output based on the extracted features. Similar to the encoder, it also consists of multiple sets of 3x3 convolutional layers. However, after each set, the decoder performs upsampling on the current feature set while halving the number of channels, aiming to restore the spatial resolution of the features lost during the encoding phase.

One characteristic of this model is the presence of skip connections between the encoder and decoder. These connections copy features from different parts of the encoder and merge them into symmetric parts of the decoder. This means that subsequent convolutional layers can operate on features from both the encoder and decoder. In semantic segmentation, the features of decoder contain rich semantic information, while the encoder contains richer spatial information. Therefore, their combined application can lead to precise pixel-level segmentation. When this model is applied to pixel-wise regression tasks, it also benefits from this advantage.

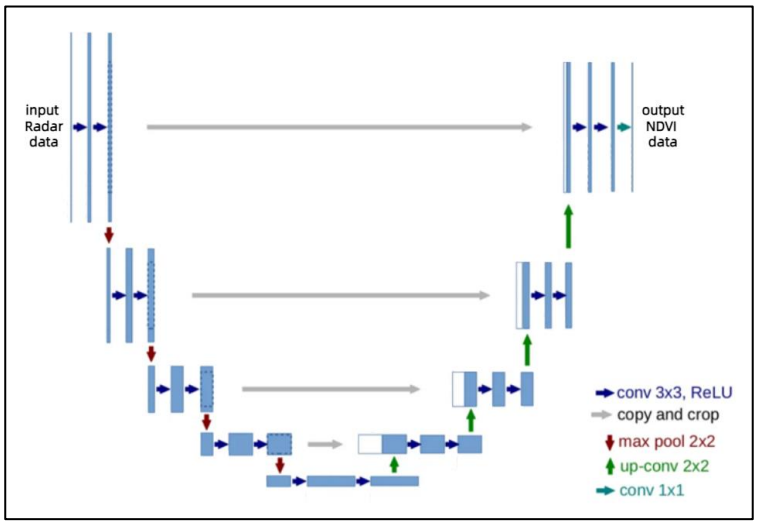

Figure 4. U-net structure (Ronneberger et al. (2015))

2.3.1.2 Training data groups

To verify the impact of different input data on model training, this study designed a total of 9 training datasets and trained the model accordingly. The composition of each dataset is shown in Table 1, where NDVI images serve as the dependent variable, and SAR images along with other auxiliary data serve as independent variables. The trained models can be categorized into three types based on the SAR data used:

- The first type includes Model M3. This model solely utilized single-day dual-polarization backscatter images and an incidence angle map as input layers.
- The second category includes models M5, M51, M52, and M53. As input for these models, backscatter data from two dates (current date and 12 days prior) were utilized to provide temporal information. Model M5 was trained using backscatter images and an incidence angle map as input. Additionally, the crop identification map, and year and week information were either fully or partially added as auxiliary data, resulting in the training of models M51, M52, and M53.
- The third category includes models M7, M71, M72, and M73. In addition to the data used in the second category, dual-polarization 12-day coherence images were provided as input. Model M7 was trained using backscatter images (current date and 12 days prior), 12-day coherence images, and an incidence angle map. Similarly, crop identification map and year and week information were fully or partially added as additional input, leading to the training of models M71, M72, and M73.

Table 1. Models trained with different image groups

		Input Image types										
		NDVI	Backscatter(VH)	Backscatter(VV)	Incidence angle map	Backscatter (VH) (12 days ago)	Backscatter (VV) (12 days ago)	12-day coherence (VH)	12-day coherence (VV)	Crop identification map	Year	week
Model names	M3	√	√	√	√							
	M5	√	√	√	√	√	√					
	M7	√	√	√	√	√	√	√	√			
	M51	√	√	√	√	√	√			√	√	√
	M52	√	√	√	√	√	√			√		
	M53	√	√	√	√	√	√				√	√
	M71	√	√	√	√	√	√	√	√	√	√	√
	M72	√	√	√	√	√	√	√	√	√		
	M73	√	√	√	√	√	√	√	√		√	√

2.3.1.3 Optimization and training

For model training, this study employs the Adam method as the optimizer. Adam is a stochastic gradient descent optimization algorithm based on adaptive estimation of low-order moments, which offers advantages such as high computational efficiency and low memory requirements, making it suitable for problems involving large datasets and multiple parameters (Kingma & Ba, 2014). The initial learning rate is set to 0.001, and the learning rates for each parameter are adaptively adjusted based on the gradients. Mean Squared Error (MSE) is used as the loss function, and Mean Absolute Error (MAE) is used as the metric to evaluate the model performance (Roßberg & Schmitt, 2023). Their formulas are as follows:

$$\boldsymbol{MSE} = \frac{\mathbf{1}}{\boldsymbol{N}} \sum_{\boldsymbol{i=0}}^{\boldsymbol{(N-1)}} (\boldsymbol{y_i} - \boldsymbol{\hat{y}_i})^{\mathbf{2}} \tag{2}$$

$$\boldsymbol{MAE} = \frac{\mathbf{1}}{\boldsymbol{N}} \sum_{\boldsymbol{i=0}}^{\boldsymbol{(N-1)}} |\boldsymbol{y_i} - \boldsymbol{\hat{y}_i}| \tag{3}$$

Before training, this study conducted 5-fold cross-validation on each set of training data to determine the most suitable batch size and number of epochs. The experimental groups for batch size were set to 16, 32, and 64, while the number of epochs was set to 150. Subsequently, each model was trained based on its cross-validation results, and the optimal parameters selected are presented in Table 2.

Table 2. Parameters of training the models tested in this study.

(For model explanation see Table 1.)

Models	Batch Size	Number of epochs
M3	32	50
M5	32	70
M7	32	70
M51	32	80
M52	32	80
M53	32	70
M71	32	140
M72	32	100
M73	32	100

2.3.2. Data preparation and NDVI prediction

In this study, the training dataset contains all available data in the region of the Netherlands from 2016-2022. All images used for training are divided into 128x128 pixels to balance training efficiency and memory usage. For year and week information, the year dummy value image contains values representing the years starting from 2010, while the week dummy value image contains values representing the weeks within the current year starting from January 1st.

To ensure training effectiveness，backscatter images, crop identification map and year and week information are all normalized between 0 and 1. The formulars are as follows：

$$Backscatter_{norm} = \frac{Backscatter+35}{50} \quad (4)$$

$$Incidence\_angle_{norm} = \frac{Incidence\_angle-20}{90} \quad (5)$$

$$Code_{norm} = \frac{GEWASCODE}{7000} \quad (6)$$

$$Year_{norm} = \frac{Year}{20} \quad (7)$$

$$Week_{norm} = \frac{Week}{60} \quad (8)$$

The pixel count of various major crops in the training dataset was checked, as shown in Figure 5. Meanwhile, the pixel count of crops in the training dataset for each month was also checked to determine the temporal distribution of the data. Taking maize as an example, its pixel distribution is shown in Figure 6.

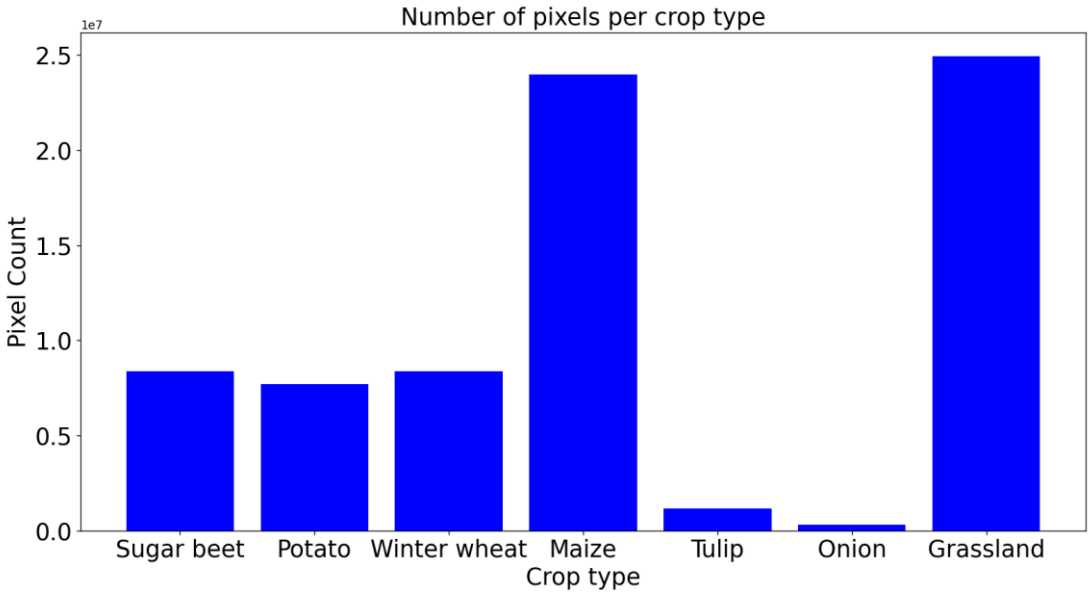

Figure 5. Number of pixels per crop type in the training dataset

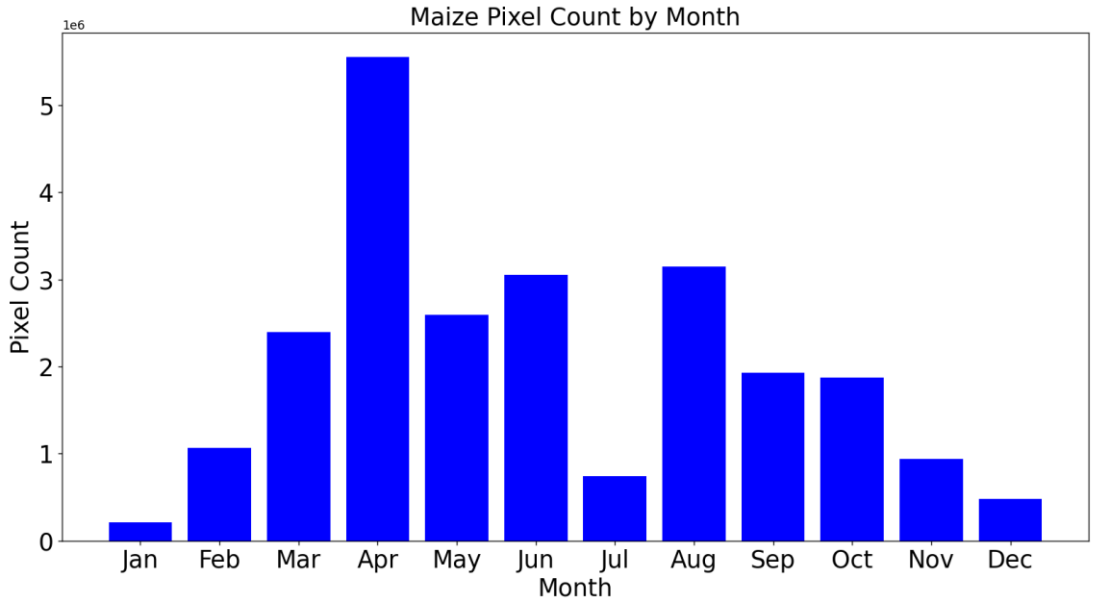

Figure 6. Maize pixel count in the training dataset by month

The dataset used for prediction included all available Sentinel-1 images from the year 2022 along with auxiliary data (crop identification map and year and week data). Before prediction, all images were normalized to a range of 0 to 1 and cropped to the Flevopolder region. Subsequently, the images were segmented into 128*128 pixel patches with a stride of 64 pixels. To reduce the memory load, 1000 batches were processed at a time for prediction. After predicting NDVI using the trained model, the NDVI values of all patches were summed up at their respective positions, and the mean was calculated between the patches to obtain the final NDVI, resulting in the predicted NDVI images.

2.3.3. Time series creation

To investigate the performance of each model in reconstructing NDVI time series, several major crops within the study area were selected, and their parcel-level NDVI time series were reconstructed. The crops can be classified into three categories:

- Full canopy crop: This category includes sugar beet, silage maize, consumption potato, and winter wheat. These crops have a fully developed canopy that covers the ground without significant visible bare soil after a certain period of growth. Winter wheat is a winter crop typically sown in late September and harvested around June or July of the following year (around the 200th day of year), while the other crops are summer crops planted in April or May and harvested around August or September of the same year.
- Half canopy crop: This category includes tulip and onion. These crops have a canopy that does not fully cover the ground throughout the growth cycle, resulting in some areas of bare soil. Both tulip and onion are summer crops, but tulips have an earlier growth cycle compared to other summer crops (approximately between the 80th and 200th day of the year).
- Grassland: This category includes both permanent and temporary grasslands. The primary agricultural activity in grassland parcels is mowing events. Since mowing only removes a certain length of grass rather than all of it, there is a persistent canopy cover in grassland parcels over time.

The first step in reconstructing the NDVI time series is to select and extract parcels of different crops within the study area. The parcel boundary map provided by WENR contains information about the land use type and crop species of each parcel, which can be used to extract parcels for each crop. For full canopy and half canopy crops, this study extracted parcels based on the GEWASCODE field for each crop. For grassland, since there is not much difference between the

two types of grassland, this study extracted the parcels of both into one category based on the CATEGORY field.

For each parcel, this study calculated the average NDVI value of all pixels corresponding to the area in the NDVI image and stored it as the NDVI value for that parcel. By performing this operation on all predicted NDVI images, parcel files containing NDVI values for multiple dates were created for each crop. Subsequently, NDVI time series for each parcel were generated based on this information. This study also performed this operation on the reference Sentinel-2 NDVI images to generate the reference NDVI time series. During the experiments, it was observed that the time series generated by combining data from two Sentinel-1 overpasses exhibited numerical fluctuations compared to those generated using data from a single overpass. To ensure the quality of the reconstructed time series, this study only used Sentinel-1 data from the central overpass to reconstruct the NDVI time series.

2.3.4. Validation

2.3.3.1 Validation on average time series

For the same type of crop, there is generally a relatively uniform growth cycle. To assess the overall quality of the reconstructed NDVI time series, the predicted NDVI time series and the reference NDVI time series of all parcels were averaged. Subsequently, this study performed linear interpolation on the average time series and assessed the quality by calculating R-squared (R^2), Root Mean Squared Error (RMSE) and percent bias (PBIAS). However, for grassland, due to variations in the timing and frequency of mowing across parcels throughout the year, averaging the time series would not be meaningful. Therefore, this study selected the reconstructed NDVI time series for several plots and directly compared them with reference NDVI to evaluate their performance.

R^2 is a metric used to assess the goodness of fit of a model, with the value indicating the fraction of the observed variance in the data that is explained by the model. A value closer to 1 indicates a better fit of the model to the data, while negative values indicate that the average reference value provides a better prediction than the model. Its formula for calculation is as follows:

$$SS_{res} = \sum_{i=1}^{n}(y_i - \hat{y}_i)^2 \tag{9}$$

$$SS_{tot} = \sum_{i=1}^{n}(y_i - \bar{y})^2 \tag{10}$$

$$R^2 = 1 - \frac{SS_{res}}{SS_{tot}} \tag{11}$$

y_i = NDVI value of the reference observation

$\hat{y}_i$ = NDVI value of the prediction of observation

$\bar{y}$ = mean of y_i

RMSE is an error metric that quantifies the combined effect of random and systematic effects (bias). It is commonly used to assess the estimation performance using a single metric. It can be calculated using the following formula:

$$RMSE = \sqrt{\frac{1}{N}\sum_{i=1}^{n}(y_i - \hat{y}_i)^2} \tag{12}$$

PBIAS can be used to measure the average tendency of simulated values to be greater than or less than observed values. The optimal value is 0, with positive values indicating overestimation and negative values indicating underestimation. Its formula is as follows:

$$PBIAS = \frac{\sum_{i=1}^{n}(\hat{y}_i - y_i)}{\sum_{i=1}^{n} y_i} \times 100\% \tag{13}$$

2.3.3.2 Validation on the results of adjusted Cropmarkers algorithm

Cropmarkers algorithm is a Python algorithm developed by WENR for cropland monitoring. It imports NDVI and VV coherence time series of all parcels in the Netherlands and estimates important arable operation dates such as ploughing, seeding, and harvest. Additionally, the algorithm predicts the dates of key nodes in the crop growth cycle, including emergence, closure, and transition (Figure 7), by fitting an S-curve to the NDVI time series. The algorithm distinguishes between summer and winter crops. Winter crops include winter wheat, winter barley, and triticale, while the rest are summer crops. The algorithm is not applicable to vegetables, fruits, grasslands, and bare soil.

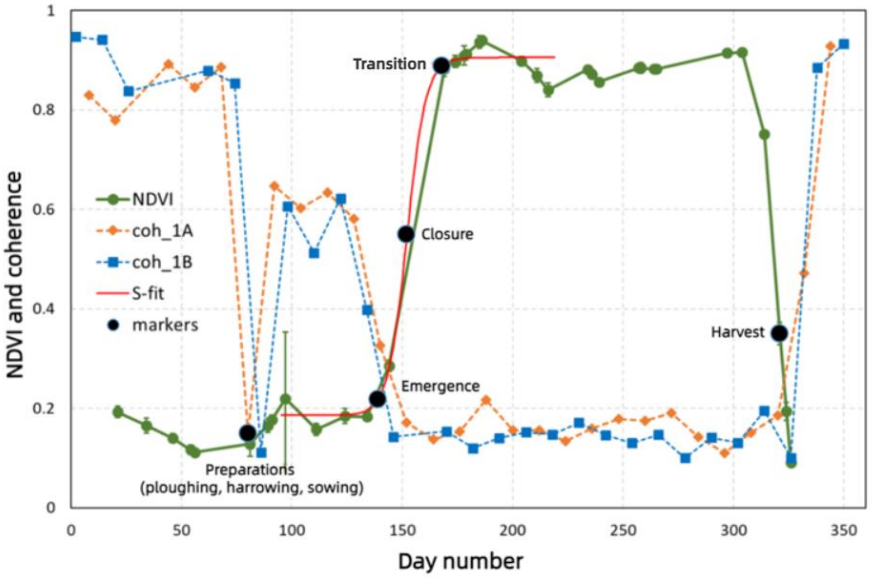

Figure 7. Example application of applying the Cropmarkers algorithm to a beet field (Groenmonitor, n.d.)

This study modified the Cropmarker algorithm to only require the NDVI time series of each parcel as input, without the need for coherence time series. The modified algorithm is applied to the reconstructed NDVI time series and detects the dates of emergence, closure, transition, and harvest for summer crops, as well as the harvest date for winter crops. Where closure indicates that the crop canopy has fully covered the soil, and transition means the critical point when the crop changes from growth to fruit development. After this node until the maturity or harvest of the crop, all solar energy will be used for fruit development. The details and decision processes of the algorithm can be found in Appendix 7.1.

This study validates the results obtained using the adjusted Cropmarkers algorithm by comparing them with the Cropmarkers reference data provided by WENR. After matching the results of each parcel with the reference data based on parcel number, Mean Absolute Error (MAE), RMSE and PBIAS are calculated to evaluate the results.

3. Results

3.1. Comparison between predicted NDVI images

Figure 8 presents the NDVI images predicted by models M3, M5, and M7 using Sentinel-1 SAR data from August 3, 2022, alongside the reference Sentinel-2 NDVI image. The grayscale range of the images is 0-1, with lighter colors indicating higher NDVI values. From the figure, it can be observed that the spatial details of the images predicted by model M3 are severely lost, resulting in overall poor prediction quality. Models M5 and M7 demonstrate generally good prediction quality. This indicates that multi-temporal backscatter images provide more effective information for model learning compared to single-day backscatter images, while the addition of coherence data does not significantly improve the predictive performance of the model at the spatial scale. Upon inspection, the predicted images by model M3 are generally blurry and fail to distinguish between different NDVI values among parcels, showing generally poor quality compared to the results of the other models. Therefore, in this study, model M3 is excluded, and the remaining eight models are chosen for the reconstruction of the NDVI time series.

Figure 8. NDVI images predicted by model M3, M5, M7 and the reference NDVI image (from left to right)

3.2. Validation on reconstructed NDVI time series

3.2.1. Full canopy crop

Figure 9 displays the comparison between the reconstructed average NDVI time series based on model M51 and the reference NDVI time series. It can be observed that while the reconstructed NDVI time series exhibit some numerical fluctuations during spring and winter, they overall capture the general trend of NDVI values throughout the growing cycle of full canopy crops well. For sugar beet, the reconstructed time series closely aligns with the reference time series in terms of the timing, magnitude, and peaks of NDVI growth and decline. For potato (consumption) and winter wheat, the model effectively predicts NDVI during the crop growth period and peak NDVI period as they mature. However, there is some prediction error during the crop harvest period, characterized mainly by a delayed NDVI decrease and overall higher predicted values compared to the reference time series. For maize, the peaks of reconstructed NDVI time series are lower than the reference NDVI time series, and the model also exhibits some errors in predicting the decline phase of NDVI.

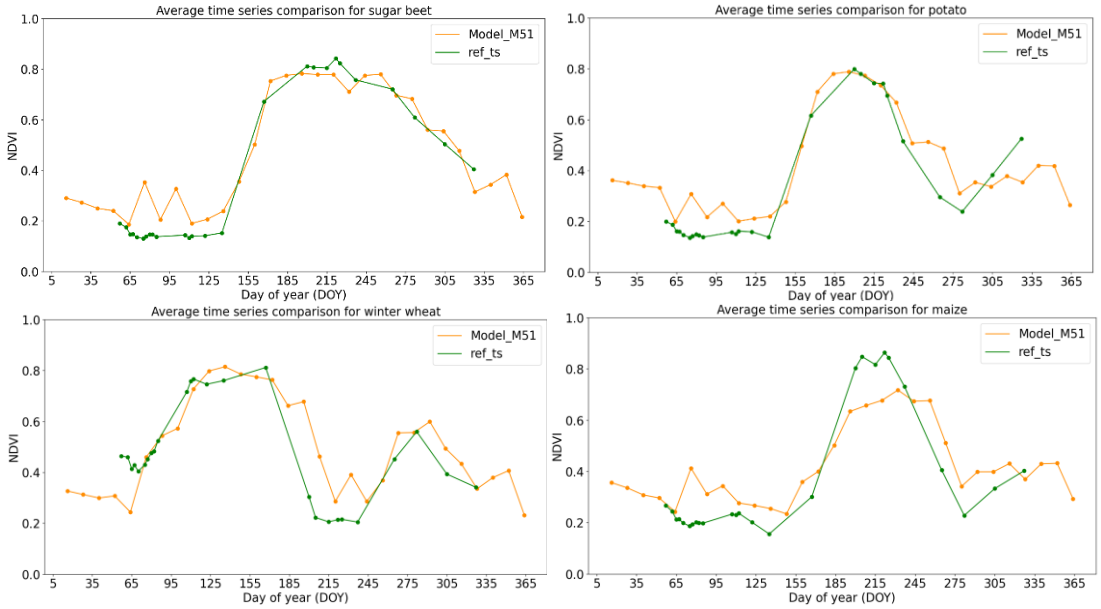

Figure 9. NDVI time series of full canopy crop reconstructed by model M51 (From left to right and top to bottom, the sequence is sugar beet, potato, winter wheat and maize)

Table 3 displays the quality assessment results of the average NDVI time series of full canopy crops reconstructed by the eight models in this study. It is observed that the models perform best in predicting sugar beet time series, with all models achieving R^2 values of around 0.9, indicating a high correlation between the reconstructed and reference time series, and a low RMSE of 0.9. The potato and maize time series have average R^2 values around 0.75 and similarly low RMSE. Winter wheat time series exhibit lower R^2 values compared to the other three crops, averaging only around 0.6, but the RMSE is not significantly higher than that of the other three crops, and the PBIAS is comparable. This may be due to the more pronounced delay in the decline of NDVI for winter wheat. It is worth noting that all models exhibit positive PBIAS values for each crop, indicating an overall tendency for models to overestimate the NDVI time series.

Among all the models, NDVI time series predicted by model M51 exhibit the highest overall R^2 and the smallest RMSE and PBIAS. Compared to Model M5, its overall performance is better, indicating that the combination of crop identification maps and year and week information can provide more useful data for the U-net model. Similarly, model M71 shows better overall performance compared to model M7, which confirms this point. However, models M52 and M53 perform worse than model M5. Compared to model M7, models M72 and M73 do not demonstrate overall better metrics as well, indicating that the separate use of crop identification maps and year and week dummy value images in model training does not provide much benefit for full canopy crops. Compared to models M7, M71, M72, and M73, models M5, M51, M52, and M53 generally have better evaluation metrics, showing more accurate NDVI prediction capabilities. This also suggests that the addition of 12-day coherence images does not help the U-net model capture more useful information during training.

Table 3. Validation of average NDVI time series for full canopy crop by each model

Crop type	Models / Matrices	M5	M7	M51	M52	M53	M71	M72	M73
Sugar beet	R^2	0.90	0.88	0.92	0.88	0.91	0.91	0.90	0.88
	RMSE	0.08	0.09	0.08	0.09	0.08	0.08	0.08	0.09
	PBIAS	3.66	7.83	6.93	13.47	9.56	10.66	11.59	7.28
Consumption Potato	R^2	0.81	0.67	0.87	0.76	0.68	0.78	0.76	0.7
	RMSE	0.1	0.13	0.08	0.11	0.12	0.1	0.11	0.12

	PBIAS	15.64	18.67	10.73	20.53	25.29	19.87	20.72	23.1
Winter wheat	R^2	0.57	0.57	0.65	0.54	0.53	0.65	0.67	0.53
	RMSE	0.12	0.12	0.11	0.13	0.13	0.11	0.11	0.13
	PBIAS	9.1	10.67	7.01	12.55	8.55	10.81	8.28	9.77
Silage maize	R^2	0.82	0.8	0.77	0.73	0.69	0.79	0.75	0.7
	RMSE	0.09	0.1	0.11	0.12	0.12	0.1	0.11	0.12
	PBIAS	9.67	14.44	9.39	19.1	19.93	16.42	13.07	18.58

3.2.2. Half canopy crop

Figure 10 depicts the comparison between the time series of half canopy crops reconstructed by Model M51 and the reference time series. In the tulip time series, only the first growth cycle corresponds to the growth cycle of tulips. It can be observed that the trend of NDVI changes can still be predicted relatively well. However, compared to full canopy crops, the time series of half canopy crops generally exhibit overestimation during the crop growth cycle. Additionally, the time series of onions also show a noticeable delay in the decline of NDVI.

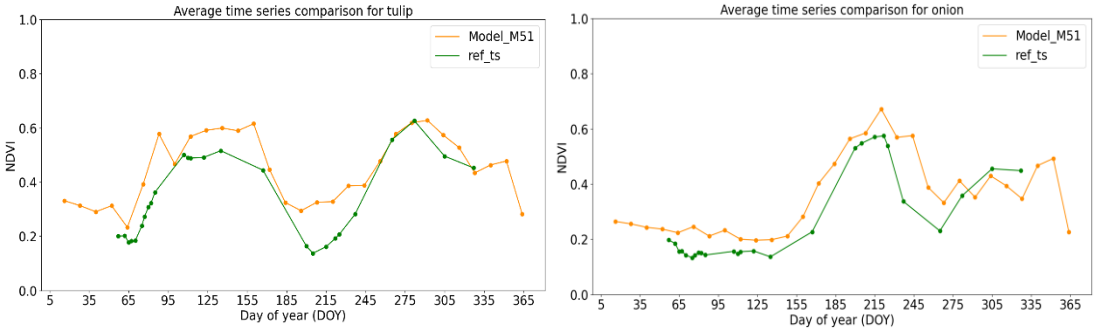

Figure 10. NDVI time series of half canopy crop reconstructed by model M51 (From left to right, the sequence is tulip and onion)

Table 4 presents the quality assessment results of the NDVI time series reconstructed by the eight models for half canopy crops in this study. It can be observed that compared to full canopy crops, the models achieved relatively lower R^2 and higher PBIAS and RMSE values in predicting the time series of half canopy crops. This indicates that the predicted NDVI time series have insufficient explanatory power for the reference time series and overall exhibit a more pronounced tendency to overestimate.

Comparing model M5 with M51, and model M7 with M71, it can be observed that models M51 and M71, which utilize crop identification map and year and week information, achieve a significant improvement in R^2 compared to M5 and M7. Additionally, there is a certain decrease in RMSE and PBIAS, indicating an improved predictive capability of the models for NDVI. Models M52 and M72 demonstrate better ability in predicting onion time series compared to M5 and M7, however, there is no improvement in tulip prediction, suggesting that adding crop identification map solely only helps in predicting onion time series. On the other hand, models M53 and M73 show worse performance in comparison to M5 and M7, indicating that using year and week dummy value images alone does not enhance the models ability for NDVI time series prediction of half canopy crops. Comparing models M5, M51, M52, M53 with models M7, M71, M72, M73, it can be observed that similar to full canopy crops, the addition of 12-day coherence images does not significantly improve the ability of the U-net model to predict NDVI time series for half canopy crops.

Table 4. Validation of average NDVI time series for half canopy crop by each model

Crop type	Models / Matrices	M5	M7	M51	M52	M53	M71	M72	M73
Tulip	R^2	0.29	0.35	0.56	-0.03	-0.12	0.51	0.35	0.26
	RMSE	0.12	0.11	0.09	0.14	0.15	0.1	0.11	0.12
	PBIAS	22.91	21.66	18.97	32.33	31.78	20.78	25.42	25.19
Onion	R^2	0.2	-0.01	0.53	0.67	-0.04	0.4	0.35	-0.02
	RMSE	0.13	0.14	0.1	0.08	0.15	0.11	0.11	0.14
	PBIAS	33.25	40.44	22.19	9.79	41.09	26.72	30.77	43.42

3.2.3. Grassland

Figure 11 illustrates two parcel-level NDVI time series reconstructed based on models M5 and M51. It can be observed that the reconstructed NDVI time series exhibit significant discrepancies compared to the reference NDVI time series, and model M51 does not perform better than model M5. In the reference time series, there are multiple rapid declines in NDVI, most of which are caused by mowing events. However, these events cannot be well predicted in the reconstructed time series. Additionally, the reconstructed NDVI time series exhibit some numerical fluctuations, which pose a risk of being misinterpreted as mowing events in practical applications such as mowing detection using NDVI time series. Therefore, the current models trained in this study have limited applicability to grasslands.

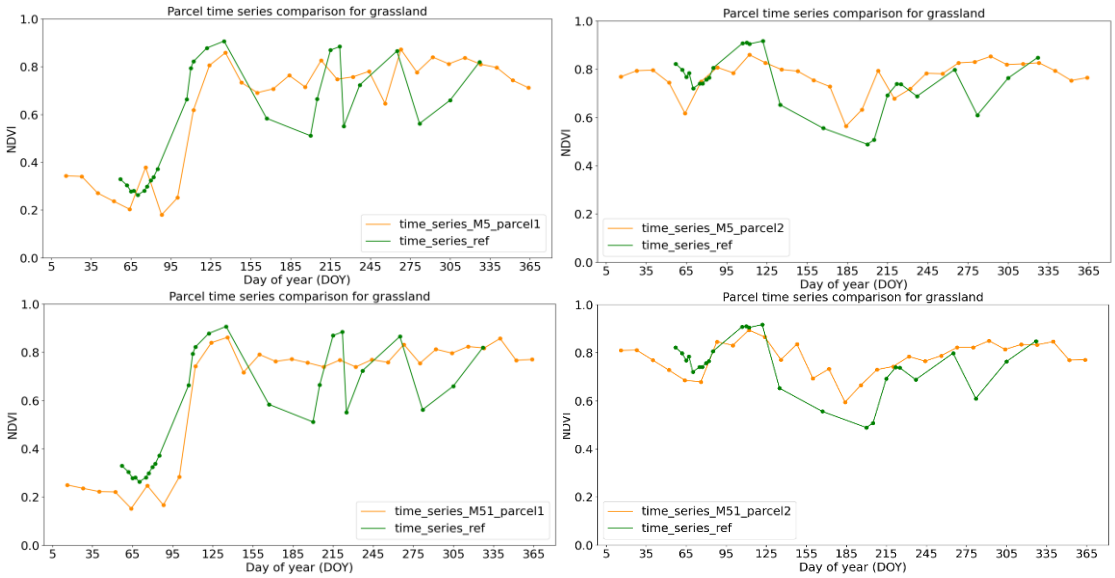

Figure 11. Two parcel NDVI time series of grassland reconstructed by model M5 (upper) and M51 (lower)

3.3. Validation on results of Cropmarkers algorithm

Figure 12 shows the MAE, RMSE, and PBIAS of the reconstructed NDVI time series of full canopy crop obtained after applying the Cropmarkers algorithm for each model. Detailed results are provided in the appendix 7.2. From the figure, it can be observed that there is not much difference in the errors obtained when detecting the occurrences of crop emergence, closure, and transition for each crop type. The average deviations for emergence and closure predictions range between 5-10 days. For transition predictions, it ranges between 10-15 days. There is a tendency for overestimation in estimating the emergence date and underestimation for closure and transition

dates. In predicting the occurrence of harvest, the results are varied among crop types. The reconstructed NDVI time series for maize and winter wheat perform better on Cropmarkers compared to the other two crops. Maize shows a very small PBIAS, indicating minimal bias in the prediction results, with errors primarily originating from random error sources. Winter wheat, on the other hand, exhibits a higher positive PBIAS, indicating a tendency to overestimate the harvest date. Sugar beet and potato showed worse results, with both having a small PBIAS and higher MAE and RMSE, which indicated that the errors were mainly random. None of the models exhibits a consistently stronger performance over the others.

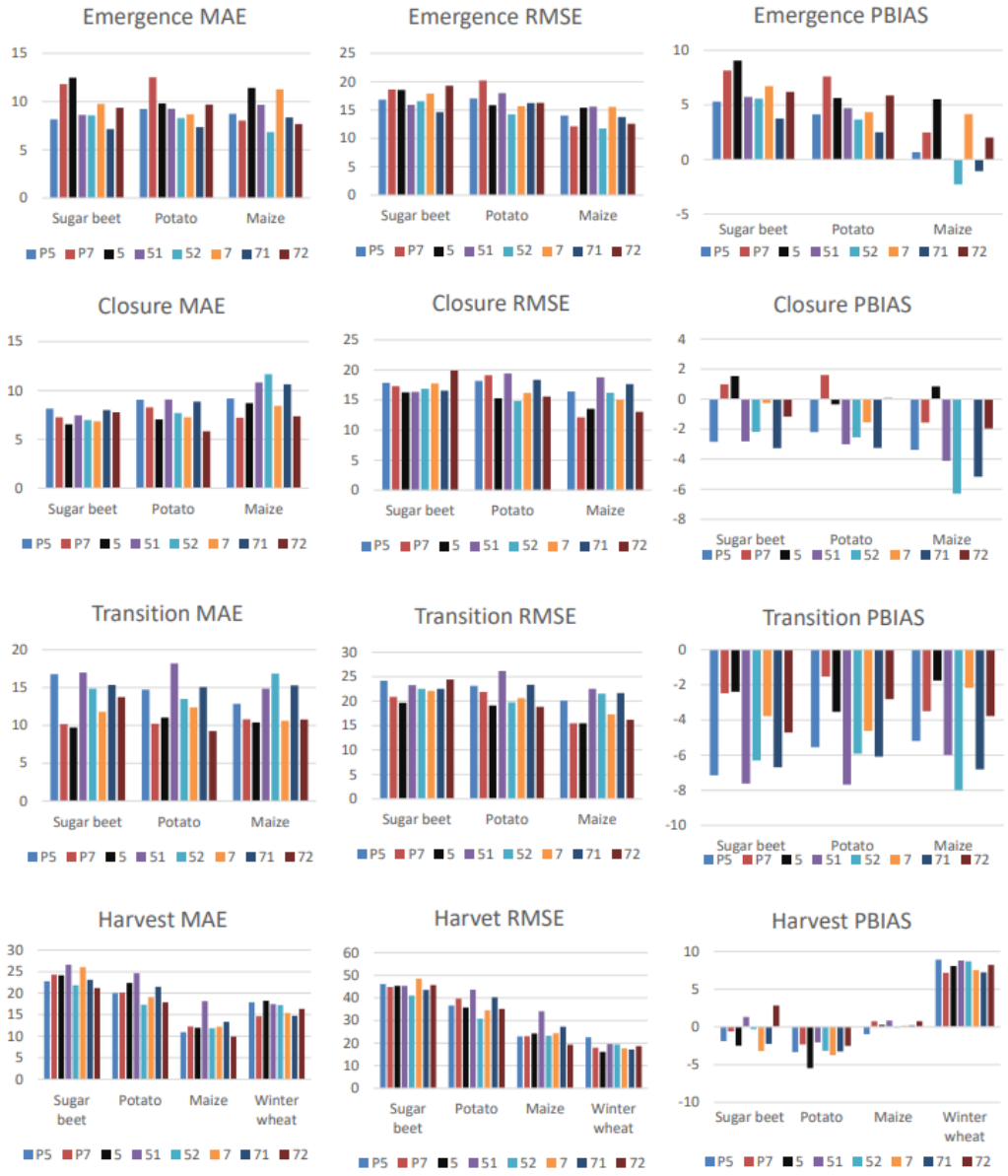

Figure 12. Validation results of Cropmarkers algorithm on full canopy crop

Figure 13 shows the results for half canopy crops. It can be observed that the overall performance of the reconstructed NDVI time series for tulip is notably worse than that of onion, with high errors in the detection of the four phenological stages. And based on the obtained PBIAS values, there are large biases in the predictions.

Figure 14 illustrates a comparison of the results distribution for the crop emergence predicted by the Cropmarkers algorithm based on the reconstructed time series for tulip and onion. It can be observed that a portion of the results shows significant deviations.

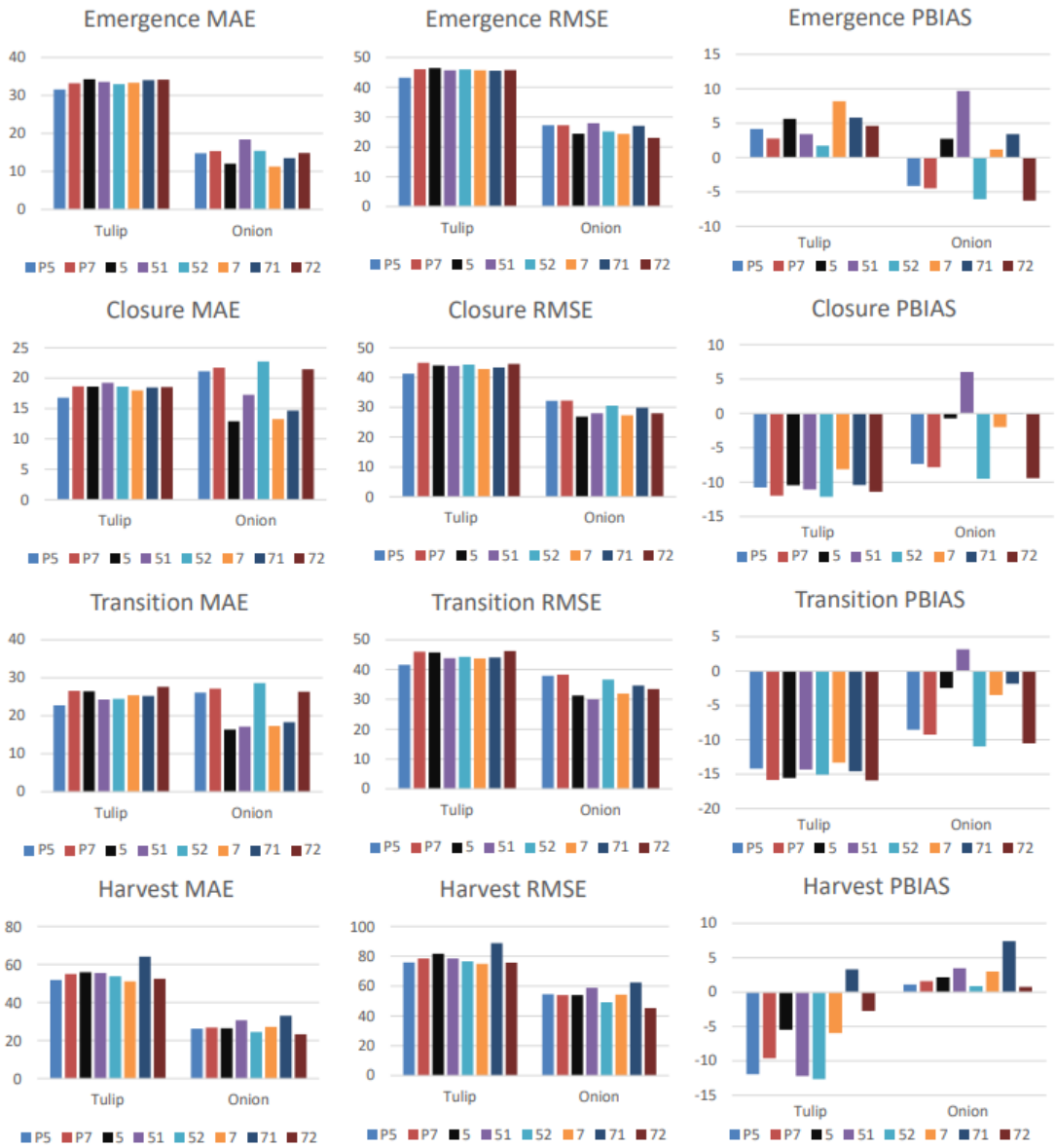

Figure 13. Validation results of Cropmarkers algorithm on half canopy crop

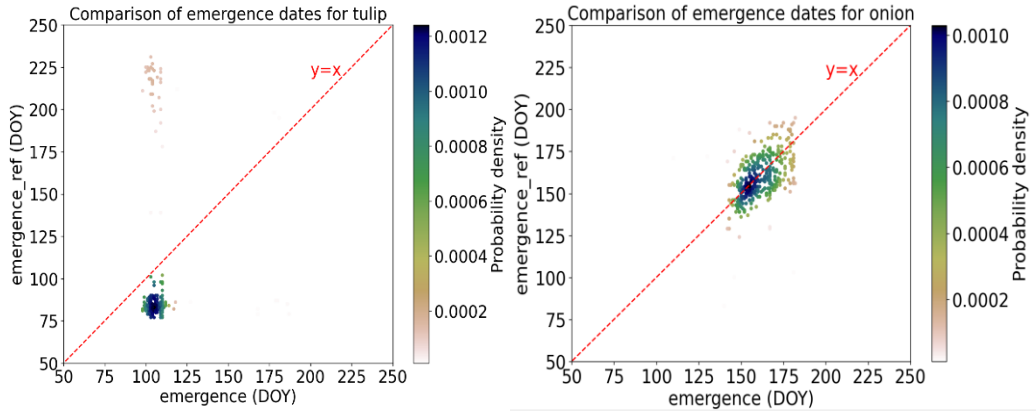

Figure 14. Scatter plot of Cropmarkers results for half canopy

(left: tulip, right: onion. X-axis is predicted Doy, Y-axis is reference Doy. The color of points represents probability density to show point distribution)

4. Discussion

4.1. Results for full canopy crops

In the results section, this study discusses the applicability of various trained models in reconstructing NDVI time series. For full canopy crops, the U-net model yields good prediction results. The NDVI time series during crop growth can be accurately simulated, demonstrating good applicability. Model M51 achieved the best evaluation metrics, indicating that combining crop identification, year, and week information provides consistently good results, while the addition of 12-day coherence images did not benefit the model.

In the reconstructed NDVI time series, it can be observed that the model exhibits some bias in predicting NDVI during the NDVI declining phase of the crop growth cycle. This problem is most evident for maize, potato, and winter wheat. One possible reason for this is the ripening process of the crops. As the fruits gradually mature, the leaves of the crops begin to age, accompanied by a reduction in chlorophyll and water content, leading to a decrease in the green vegetation cover and consequently a decrease in NDVI values in Sentinel-2 imagery. During this stage, the vegetation canopy structure and moisture does not change significantly, resulting in small changes in Sentinel-1 backscatter images and 12-day coherence images, which are sensitive to structural changes. This leads to the insignificant changes in the reconstructed NDVI time series. Chen et al. (2023) demonstrated that SAR signals become unstable and noisy during the maturation stage of crops, which may also contribute to this problem. When the predicted NDVI begins to decline, it often indicates the maturity of crop physical structure or the start of harvesting.

In addition, the reconstructed NDVI time series of maize has peaks that are lower than the reference NDVI time series. This is probably due to the uneven distribution of pixel counts for maize fields in the training dataset across different months. Figure 6 illustrates the distribution of maize pixels in the training dataset for each month, showing a significantly lower pixel count in July compared to other months of the growing season. The underestimation of NDVI values mainly occurs in July (Figure 9), supporting this hypothesis.

Through the PBIAS values in Table 3, it can be observed that almost all models exhibit positive PBIAS across each crop type, indicating a tendency for overestimation in the reconstructed time series. One possible reason for this phenomenon is the relative instability of the predictive performance of the model outside the crop growth cycles. During spring and winter, precipitation, freezing, flooding, and other factors may induce changes in soil moisture and structure, causing fluctuations in radar imagery, which could in turn lead to variations in NDVI predicted by the model. As most parcels are bare during these periods, actual NDVI levels are low, so the fluctuation of NDVI appears as an overestimation. Additionally, the model overestimates during the period of NDVI decrease, which is a contributing factor.

Based on the results obtained from the application of the Cropmarkers algorithm, the reconstructed NDVI time series in this study demonstrate relatively good performance in predicting the occurrences of emergence, closure, and transition. When predicting harvest occurrence, there are differences in the results obtained for different crops. Sugar beet and potato show relatively large random errors, indicating that while the model performs well on average time series, there are still differences in the predictive quality of NDVI time series for different parcels. Winter wheat and maize have overall small errors, but the composition of errors is different. Error of maize mainly comes from random errors with very small bias, demonstrating the best performance among all crops. On the other hand, results of winter wheat show a tendency for overall overestimation, possibly due to the more pronounced delay in NDVI decline time in the reconstructed NDVI time series.

4.2. Results for half canopy crops

The model trained in this study performs overall worse in predicting the NDVI time series of half canopy crops compared to full canopy crops. The predicted NDVI is significantly higher than the reference NDVI time series. This is probably due to that half canopy crop parcels are less represented in the training data. Figure 5 illustrates the number of pixels for each crop parcel in

the training dataset, and it can be seen that the tulip and onion only take up a very small portion of the training data. As a result, the U-net model mostly captures the relationship between NDVI and SAR data of full canopy crops during training, while lacking sufficient training data for half canopy crops. When predicting NDVI, the model interprets the changes in SAR image values for half canopy crop parcels based on the relationship between NDVI and SAR data for full canopy crops. Since full canopy crops generally have higher NDVI values throughout the growth cycle, this leads to an overestimation of the NDVI time series for half canopy crops by the model. Model M51 still achieves the best evaluation metrics for the reconstructed NDVI time series, indicating that the auxiliary data such as crop identification maps added to training dataset helps the U-net model distinguish between different crops to some extent, contributing to addressing this issue. However, more effective solutions are still needed. The 12-day coherence data still does not provide benefits for the model training.

On the results obtained using the Cropmarkers algorithm, half canopy crops generally perform worse compared to full canopy crops, which is attributed to the insufficient training of the model on half canopy crops. Tulip results show a high systematic error, as can be seen in Figure 14, where results for some parcels are underestimated. Since tulips have a relatively early growth cycle compared to other crops, after the harvest of tulips, other types of crops may be planted in the parcels. In the Cropmarkers reference data, the recorded timings for phenological stages for these parcels might belong to the crops planted after tulips (for instance, most of the reference dates for incorrectly predicted emergence dates are around day 225, corresponding to the start of the second growth cycle in Figure 10), leading to this issue.

4.3. Results for grasslands

From the first parcel NDVI time series (left) in Figure 11, it can be observed that the NDVI of this parcel increases from around 0.3 to above 0.8 from March to May. One possible reason for this phenomenon is that the parcel was previously used for other purposes and was only converted to grassland in 2022. The period from March to May is when grass grows to its normal canopy coverage. During this process, the model performs well in predicting NDVI changes. In the later part of that year, the NDVI remains relatively high, indicating the persistent presence of grassland canopy coverage. The predictive performance of models during this period is poor. The main agricultural activity in the grassland parcel is mowing, which only cuts a certain length of grass rather than all of it, resulting in canopy cover always being present. Compared to the changes in surface structure caused by transitioning from bare soil to significant vegetation cover, the changes caused by mowing are relatively small, and the grassland canopy structure remains relatively similar before and after mowing. This may have brought difficulties for the learning and discrimination of the U-net model, leading to this problem.

4.4. Comparison with literature

Mohite et al. (2020) employed tuned Support Vector Regression (SVR) and tuned Random Forest Regression (RFR) to reconstruct the NDVI time series based on Sentinel-1 data for rice, cotton, banana, and turmeric crops. The first three crops are full canopy crops, while turmeric is a half canopy crop. In their study, the best performing RFR achieved R^2 values of 0.79, 0.76, 0.69 for rice, cotton, banana respectively, with RMSE values of 0.08, 0.09, 0.11, and obtained an R^2 value of 0.71 with an RMSE of 0.12 for turmeric. Compared to this study, the method employed in my study yielded overall better R^2 results for full canopy crops, demonstrating better performance over regular machine learning algorithms. However, for half canopy crops, my results were worse than that of this study, which is due to the insufficient training of models on half canopy crops. Chen et al. (2023) integrated SAR raw data features, various radar vegetation index features, and temperature-related data to regress NDVI time series for maize and soybean using a random forest model. Across the reconstructed NDVI time series covering the entire growth cycle, this method achieved an R^2 of 0.725 and RMSE of 0.145 for maize, and an R^2 of 0.437 and RMSE of 0.269 for soybean, which is a half canopy crop. Compared to this study, my method yielded better results for maize and similarly performed well for the half canopy crop, demonstrating better applicability. Notably, this study demonstrated that both radar-related vegetation indices, as well as temperature-related data, can provide gains for model training, highlighting the potential of using multisource data to improve model performance.

In studies employing deep learning models, image-based NDVI prediction tends to focus more on spatial scale validation, with less emphasis on the temporal scale. While time-series-based NDVI prediction are more validated on the temporal scale. Zhao et al. (2020) utilized the MCNN-Seq model based on SAR time series to predict NDVI time series, achieving R^2 values of 0.9409, 0.9824, 0.9157, 0.9749, and 0.7018 for onion, winter wheat, maize, sugar beet, and alfalfa respectively. Compared to their study, the results obtained in my research were relatively worse. However, it is worth noting that their validation was field-specific, thus the performance in broader areas remains uncertain. Garioud et al. (2021) employed the SenRVM model with a recurrent neural network (RNN) architecture, also regressing NDVI time series based on SAR time series. They trained the model on a single-class dataset containing only crop data, achieving an average R^2 of 0.95 and RMSE of 0.06 for predicted NDVI time series of crop parcels, which are better than my results as well. Through these comparisons, time series-based methods may have an advantage in capturing temporal features within complete time series, leading to better overall prediction performance. However, compared to the method used in this study, it lacks flexibility and cannot perform real-time supplementation of NDVI time series.

4.5. Suggestions for future development

This study only validated the reconstructed NDVI time series of various crop plots within the study area for the year 2022. As factors such as overall weather conditions and moisture levels may vary across different years and could influence the results, it is necessary to validate the methods used in this study across multiple years. Additionally, expanding the study area further would help to further verify the generalizability of the U-net model.

The combined use of multi-source data in training deep learning models has shown great potential for improving model performance. Therefore, it is advisable to jointly use different data sources in the training dataset. For example, adding RGB images may enhance the prediction of the U-net model during crop ripening stages, and vegetation index data related to radar may help the model better learn the relationship between SAR data and NDVI, etc. Additionally, incorporating data from more temporal phases might enable the model to capture more information on time scales during training, thereby improving overall prediction performance. So, this is also a point worth trying.

In this study, the overall prediction performance of the U-net model on NDVI time series of half canopy crops was poor due to their low representation in the training data. Therefore, future research should focus on balancing the proportions of different crop parcels in the training data. It is also worth trying to create separate training data for different types of crops, which may improve the model performance when applied to specific crop types. It is also important to ensure that the training data is evenly distributed on the time scale during the crop growth cycle to avoid situations where predicted values are lower than reference values during certain periods.

5. Conclusion

This study investigated a method for reconstructing NDVI time series based on the U-net model. The performance of the trained models on different crops and the influence of different input data combinations on the model performance were evaluated. Additionally, the usability of the reconstructed time series for detecting crop phenological stages was validated.

The model performed best on full canopy crops, demonstrating good usability, while the results on half canopy crops were relatively poor. This was attributed to the disproportionate representation of different crops in the training dataset, leading to insufficient training of the model on half canopy crops. Therefore, it is recommended to balance the proportions of different crops in the training data to improve model performance. The model showed poor predictive performance for grasslands. The change in vegetation canopy caused by mowing, the main agricultural activity of grassland, is smaller than the process of other crops from bare soil to crop canopy coverage, which makes accurate prediction of the model difficult. Specialized training of the U-net model using a training dataset containing only grassland parcels may improve prediction quality.

In terms of the use of input data, multi-temporal backscatter images significantly improve the performance of the model compared to single-day backscatter images, indicating the necessity of providing temporal information for model training. However, the joint use of 12-day interferometric coherence images did not improve performance. The combined use of a crop identification map and year and week data provided an overall improvement in the performance of the U-net model, which demonstrates the potential of combining data from multiple sources to improve model performance, so this is worthy of further exploration.

For crop phenological stage detection, the NDVI time series reconstructed by the method in this study achieved relatively good results in predicting crop emergence, closure, and transition, with varying prediction performance for harvest among different crops.

In summary, the method used in this study can effectively reconstruct NDVI time series, providing valuable information for crop growth monitoring, with great potential for performance improvement. With the increasing importance of agricultural production monitoring, it can provide rich information for agricultural management, assisting managers in making relevant decisions to achieve more efficient and secure agricultural production, thereby contributing to the goal of global agricultural output growth.

6. Reference

Cao, R., Chen, Y., Shen, M., Chen, J., Zhou, J., Wang, C., & Yang, W. (2018). A simple method to improve the quality of NDVI time-series data by integrating spatiotemporal information with the Savitzky-Golay filter. Remote Sensing of Environment, 217, 244-257.

Chen, D., Hu, H., Liao, C., Ye, J., Bao, W., Mo, J., ... & Pei, J. (2023). Crop NDVI time series construction by fusing Sentinel-1, Sentinel-2, and environmental data with an ensemble-based framework. Computers and Electronics in Agriculture, 215, 108388.

Drusch, M., Del Bello, U., Carlier, S., Colin, O., Fernandez, V., Gascon, F., ... & Bargellini, P. (2012). Sentinel-2: ESA's optical high-resolution mission for GMES operational services. Remote sensing of Environment, 120, 25-36.

Eilers, P. H. (2003). A perfect smoother. Analytical chemistry, 75(14), 3631-3636.

Fan, X., Yan, C., Fan, J., & Wang, N. (2022). Improved U-net remote sensing classification algorithm fusing attention and multiscale features. Remote Sensing, 14(15), 3591.

Fieuzal, R., Baup, F., & Marais-Sicre, C. (2013). Monitoring wheat and rapeseed by using synchronous optical and radar satellite data—From temporal signatures to crop parameters estimation. Advances in Remote Sensing, 2, 162-180

Gamon, J. A., Field, C. B., Goulden, M. L., Griffin, K. L., Hartley, A. E., Joel, G., ... & Valentini, R. (1995). Relationships between NDVI, canopy structure, and photosynthesis in three Californian vegetation types. Ecological applications, 5(1), 28-41.

Gao, F., Anderson, M. C., Zhang, X., Yang, Z., Alfieri, J. G., Kustas, W. P., ... & Prueger, J. H. (2017). Toward mapping crop progress at field scales through fusion of Landsat and MODIS imagery. Remote Sensing of Environment, 188, 9-25.

Garioud, A., Valero, S., Giordano, S., & Mallet, C. (2021). Recurrent-based regression of Sentinel time series for continuous vegetation monitoring. Remote Sensing of Environment, 263, 112419.

Griffiths, P., Nendel, C., Pickert, J., & Hostert, P. (2020). Towards national-scale characterization of grassland use intensity from integrated Sentinel-2 and Landsat time series. Remote Sensing of Environment, 238, 111124.

Groenmonitor. (n.d.). Bouwland Monitoring Service [PDF file]. Retrieved May 1, 2024, from https://www.groenmonitor.nl/sites/default/files/WENR_Bouwland_Monitoring_Service.pdf.

Johnson, J. A., Runge, C. F., Senauer, B., Foley, J., & Polasky, S. (2014). Global agriculture and carbon trade-offs. Proceedings of the National Academy of Sciences, 111(34), 12342-12347.

Kingma, D. P., & Ba, J. (2014). Adam: A method for stochastic optimization. arXiv preprint arXiv:1412.6980.

Li, J., Li, C., Xu, W., Feng, H., Zhao, F., Long, H., ... & Yang, G. (2022). Fusion of optical and SAR images based on deep learning to reconstruct vegetation NDVI time series in cloud-prone regions. International Journal of Applied Earth Observation and Geoinformation, 112, 102818.

Li, S., Xu, L., Jing, Y., Yin, H., Li, X., & Guan, X. (2021). High-quality vegetation index product generation: A review of NDVI time series reconstruction techniques. International Journal of Applied Earth Observation and Geoinformation, 105, 102640.

Mercier, A., Betbeder, J., Rapinel, S., Jegou, N., Baudry, J., & Hubert-Moy, L. (2020). Evaluation of Sentinel-1 and-2 time series for estimating LAI and biomass of wheat and rapeseed crop types. Journal of applied remote sensing, 14(2), 024512-024512.

Mirzaee, S., Motagh, M., Arefi, H., & Nooryazdan, M. (2014). Classification of agricultural fields using time series of dual polarimetry TerraSAR-X images. The International Archives of the Photogrammetry, Remote Sensing and Spatial Information Sciences, 40, 191-196.

Mohite, J. D., Sawant, S. A., Pandit, A., & Pappula, S. (2020). Investigating the performance of random forest and support vector regression for estimation of cloud-free NDVI using Sentinel-1 SAR data. The International Archives of the Photogrammetry, Remote Sensing and Spatial Information Sciences, 43, 1379-1383.

Moreira, A., Prats-Iraola, P., Younis, M., Krieger, G., Hajnsek, I., & Papathanassiou, K. P. (2013). A tutorial on synthetic aperture radar. IEEE Geoscience and remote sensing magazine, 1(1), 6-43.

Pipia, L., Muñoz-Marí, J., Amin, E., Belda, S., Camps-Valls, G., & Verrelst, J. (2019). Fusing optical and SAR time series for LAI gap filling with multioutput Gaussian processes. Remote Sensing of Environment, 235, 111452.

Roßberg, T., & Schmitt, M. (2023). A Globally Applicable Method for NDVI Estimation from Sentinel-1 SAR Backscatter Using a Deep Neural Network and the SEN12TP Dataset. PFG–Journal of Photogrammetry, Remote Sensing and Geoinformation Science, 1-18.

Ronneberger, O., Fischer, P., & Brox, T. (2015). U-net: Convolutional networks for biomedical image segmentation. In Medical image computing and computer-assisted intervention–MICCAI 2015: 18th international conference, Munich, Germany, October 5-9, 2015, proceedings, part III 18 (pp. 234-241). Springer International Publishing.

Scarpa, G., Gargiulo, M., Mazza, A., & Gaetano, R. (2018). A CNN-based fusion method for feature extraction from sentinel data. Remote Sensing, 10(2), 236.

Spoto, F., Sy, O., Laberinti, P., Martimort, P., Fernandez, V., Colin, O., ... & Meygret, A. (2012, July). Overview of sentinel-2. In 2012 IEEE international geoscience and remote sensing symposium (pp. 1707-1710). IEEE.

Torres, R., Snoeij, P., Geudtner, D., Bibby, D., Davidson, M., Attema, E., ... & Rostan, F. (2012). GMES Sentinel-1 mission. Remote sensing of environment, 120, 9-24.

Turner, D. P., Cohen, W. B., Kennedy, R. E., Fassnacht, K. S., & Briggs, J. M. (1999). Relationships between leaf area index and Landsat TM spectral vegetation indices across three temperate zone sites. Remote sensing of environment, 70(1), 52-68.

Wang, J., Xiao, X., Bajgain, R., Starks, P., Steiner, J., Doughty, R. B., & Chang, Q. (2019). Estimating leaf area index and aboveground biomass of grazing pastures using Sentinel-1, Sentinel-2 and Landsat images. ISPRS Journal of Photogrammetry and Remote Sensing, 154, 189-201.

Xu, L., Li, B., Yuan, Y., Gao, X., & Zhang, T. (2015). A temporal-spatial iteration method to reconstruct NDVI time series datasets. Remote Sensing, 7(7), 8906-8924.

Zhao, W., Qu, Y., Chen, J., & Yuan, Z. (2020). Deeply synergistic optical and SAR time series for crop dynamic monitoring. Remote Sensing of Environment, 247, 111952.

7. Appendix

7.1. Details and decision processes of the modified Cropmarkers algorithm

The modified Cropmarkers algorithm takes NDVI time series of all parcels from an area as the input. The algorithm begins with data preparation, using a Whittaker filter (Eilers, 2003) to smooth the input NDVI time series. It then generates an array "d_NDVI", containing the differences between every two NDVI points, followed by creating the "sum_d_NDVI" array to record continuous decreases in NDVI values based on the "d_NDVI" array. The algorithm also creates arrays "doy_NDVI" to record the day of year (Doy) of NDVI images and "d_doy" to record the intervals between dates. The "lowest_ten" NDVI value with a numerical size of 10% is also calculated.

Crop emergence, closure and transition dates

For the detection of crop emergence, closure, and transition, the Cropmarker algorithm first determines the crop type based on the plot number. If it is a summer crop, it determines whether vegetation cover exists in each parcel during the winter (Table 5). The winter status of the parcel is then further used to detect the occurrence of ploughing (Table 6).

Table 5. Winter status judging process

Step 1	Doy < 100		
Step 2	$NDVI_{mean}$ >0.4	else	
Step 3	_	Doy < 50	
Step 4	_	$NDVI_{mean}$ >0.4	else
Winter status	Winter green	Winter green	Winter bare

Table 6. Ploughing detecting process

Step 1	Doy ⩽ 175			
Step 2	If winter status = "winter green"			If winter status = "winter bare"
Step 3	Doy of minimal d_NDVI to Doy of minimal d_NDVI + 50 days	Doy of minimal sum_d_NDVI to Doy of minimal sum_d_NDVI + 50 days		_
Step 4	NDVI_1 <0.35 or (NDVI_1<lowest_ten and $NDVI_{mean}$ < NDVI_1) (NDVI_1=Doy where d_NDVI is smallest)	NDVI_2 <0.35 or (NDVI_2<lowest_ten and $NDVI_{mean}$ < NDVI_2) (NDVI_2=Doy where sum_d_NDVI is smallest)		_
Step 5	Ploughing date1 = Doy of $(d\_NDVI)_{min}$	Ploughing date2 = Doy of $(sum\_d\_NDVI)_{min}$		_
Step 6	If both ploughing date1 and date2 exist	If only ploughing date1 exists	If only ploughing date2 exists	_
Results	Ploughing date = ploughing date1		Ploughing date = ploughing date2	No ploughing moment detected

The modified Cropmarker algorithm detects the dates of crop emergence, closure, and transition by fitting an S-curve to the NDVI time series. Based on the timing of ploughing, the algorithm determines the time range "sfit_x" of the S-curve and the indices "ix" of the data used for optimizing functions. The specific conditions and results are presented in Table 7.

Table 7. Determination of ix and sfit_x

Step 1	If ploughing exist				else
Step 2	If Doy of ploughing > 100			else	_
Step 3	Doy of ploughing to 250			_	_
Step 4	If there are more than one peak value in NDVI time series		else	_	_
Step 5	If the peak occurs after the ploughing date more than once.	else	_	_	_
Results	ix = (Doy⩾ploughing date) & (Doy⩽Doy of the earliest peak NDVI) sfit_x: From (ploughing date -5) to (Doy of the earliest peak NDVI +5)	ix = (Doy>ploughing date) & (Doy<Doy of the peak NDVI) sfit_x: From (ploughing date -5) to (Doy of the peak NDVI +5)	ix = (Doy>ploughing date) & (Doy<Doy of the peak NDVI) sfit_x: From (ploughing date -5) to (Doy of the peak NDVI +5)	ix = (Doy⩾100) & (Doy ⩽215)&(sum_d_NDVI ⩾ -0.15 sfit_x: From 95 to 220	ix = (Doy⩾100) & (Doy ⩽215)&(sum_d_NDVI ⩾ -0.15 sfit_x: From 95 to 220

The Cropmarker algorithm fits an S-curve using a sigmoid function (equation 14). Default, minimum, maximum, and standard deviation values are set for each parameter (Table 8). The algorithm first uses the Doy and NDVI data at the ix index as the dataset and employs the GN_DIRECT_L and LN_COBYLA algorithms from the NLopt library to optimize the parameters, aiming to find the optimal fit under the specified constraints. Subsequently, the optimized parameter set is used to fit the S-curve, where the date of the first 45-degree point on the curve is determined as the date of crop emergence, the date of the second 45-degree point as the date of transition, and the optimized parameter a3 as the date of crop closure.

$$Sigmoid\ Function = a0 + \frac{a1}{(1+e^{-\frac{x-a3}{a2}})} \tag{14}$$

Table 8. Parameter constraints for curve fitting (eq. 14)

parameter	a0	a1	a2	a3
Lower bounds	0.1	0.2	2	110
Upper bounds	0.3	0.75	9	200
Default values	0.2	0.7	5	160
Standard Deviation	0.05	0.05	2.5	10

Harvest of summer crop

At the time of harvest, the NDVI of a parcel often rapidly declines to a relatively low value, which the Cropmarkers algorithm primarily utilizes to identify the harvest date. Additionally, to exclude other agricultural activities such as mowing, the algorithm also considers the slope of the NDVI time series, calculated by dividing d_NDVI by d_doy. The algorithm first seeks the maximum NDVI within a period after crop closure. If crop closure is detected, the algorithm searches for the maximum NDVI within the period from the closure date to 100 days afterward. If closure is not detected, the algorithm searches for the maximum NDVI between the 150th and 250th days. If multiple maximum NDVI values are found, the interval containing the harvest occurrence is defined as from the earliest maximum NDVI date to the 360th day; otherwise, it is defined as from the maximum NDVI date to the 360th day. The specific determination of harvest is detailed in Table 9.

Table 9. Determination of summer crop harvest

Step 1	(d_NDVI < -0.2) & (NDVI < 0.5) & (slope < -0.01)	else	
Step 2	_	($sum\_d\_NDVI)_{min}$ < -0.3) & (NDVI< 0.475)	else
Step 3	_	The earliest DOY meeting the step 2 condition to 50 days after it	d_NDVI < -0.3
Step 4	_	($NDVI_{mean}$ < the earliest NDVI) | ($NDVI_{min}$ < 0.4) | (the earliest NDVI < 0.4)	The earliest DOY meeting step 3 condition to 50 days after
Step 5	_	_	$NDVI_{mean}$ < the earliest NDVI
Results	Harvest date = the earliest date meeting step 1 condition	Harvest date = the earliest date meeting step 2 condition	Harvest date = the earliest date meeting step 3 condition

Harvest of winter crop

For determining the harvest of winter crops, the Cropmarker algorithm also relies on NDVI, d_NDVI, and sum_d_NDVI combined with the slope of the time series. The algorithm first defines the date range between 150 and 250 Doy as the potential harvest period. Within this range, the algorithm assesses whether there are date indices that meet the conditions specified in Table 10. If there are no such indices, the slope is considered as 0. If there are date indices that meet the conditions and there are at least two points within the interval from the earliest date to 35 days afterward, the algorithm employs least squares fitting to estimate a linear model and calculate the slope. Otherwise, the slope is considered as 0. Subsequently, the algorithm combines the conditions specified in Table 10 with the slope to determine the occurrence of harvest, as detailed in Table 11.

Table 10. Conditions of calculating slope

Condition 1	Condition 2	Condition 3
((d_NDVI)min < -0.3) & (NDVI < 0.45)	(sum_d_NDVI)min < -0.3) & (NDVI < 0.45)	d_NDVI < -0.3

Table 11. Determination of winter crop harvest

Step 1	((d_NDVI)min < -0.3) & (NDVI < 0.45) & (slope < 2)	else	_
Step 2	_	(sum_d_NDVI)min < -0.3) & (NDVI < 0.45) & (slope < 2)	else
Step 3	_	_	(d_NDVI < -0.3) & (slope <2)
Results	Harvest date = The earliest date meeting step 1 condition	Harvest date = The earliest date meeting step 2 condition	Harvest date = The earliest date meeting step 3 condition

7.2. Validation results of applying Cropmarkers algorithm

Table 12. Validation results of applying Cropmarkers algorithm on full canopy crop

phenological stage	Matrices	Models / Crop type	M5	M7	M51	M52	M53	M71	M72	M73
Emergence	MAE	Sugar beet	8.15	11.81	12.48	8.61	8.58	9.76	7.14	9.36
		Consumption potato	9.24	12.51	9.79	9.25	8.28	8.69	7.35	9.69
		silage maize	8.73	8.02	11.43	9.67	6.83	11.27	8.35	7.68
	RMSE	Sugar beet	16.82	18.62	18.55	15.93	16.57	17.91	14.65	19.3
		Consumption potato	17.06	20.21	15.88	17.99	14.27	15.66	16.25	16.27
		silage maize	14.04	12.14	15.40	15.60	11.77	15.58	13.77	12.6
	PBIAS	Sugar beet	5.3	8.15	9.07	5.74	5.58	6.72	3.76	6.19
		Consumption potato	4.14	7.62	5.64	4.7	3.65	4.33	2.49	5.86
		silage maize	0.67	2.48	5.52	0.05	-2.29	4.16	-1.07	2.01
Closure	MAE	Sugar beet	8.13	7.25	6.53	7.45	6.97	6.84	7.98	7.77
		Consumption potato	9.04	8.28	7.03	9.08	7.69	7.26	8.86	5.83
		silage maize	9.17	7.21	8.71	10.82	11.66	8.42	10.62	7.35
	RMSE	Sugar beet	17.85	17.29	16.28	16.33	16.89	17.75	16.55	19.89
		Consumption potato	18.16	19.11	15.29	19.42	14.84	16.17	18.36	15.57
		silage maize	16.43	12.12	13.53	18.77	16.20	15.03	17.63	13.05
	PBIAS	Sugar beet	-2.84	0.98	1.54	-2.81	-2.18	-0.26	-3.27	-1.17
		Consumption potato	-2.2	1.61	-0.35	-3.01	-2.55	-1.55	-3.25	0.07
		silage maize	-3.38	-1.56	0.84	-4.11	-6.29	-0.01	-5.16	-1.96
Transition	MAE	Sugar beet	16.77	10.16	9.72	16.99	14.86	11.78	15.34	13.75
		Consumption potato	14.71	10.21	11.03	18.19	13.49	12.38	15.06	9.24
		silage maize	12.84	10.8	10.4	14.85	16.86	10.61	15.28	10.79
	RMSE	Sugar beet	24.18	20.87	19.67	23.26	22.54	22.1	22.54	24.44
		Consumption potato	23.12	21.89	19.11	26.16	19.74	20.63	23.36	18.83
		silage maize	20.1	15.46	15.47	22.53	21.54	17.31	21.67	16.2
	PBIAS	Sugar beet	-7.14	-2.48	-2.39	-7.62	-6.3	-3.78	-6.69	-4.72
		Consumption potato	-5.54	-1.53	-3.53	-7.67	-5.92	-4.62	-6.09	-2.81
		silage maize	-5.19	-3.5	-1.75	-5.99	-7.99	-2.18	-6.81	-3.77
Harvest	MAE	Sugar beet	22.78	24.29	24.15	26.62	21.83	26.06	23.1	21.21
		Consumption potato	20.03	20.13	22.38	24.64	17.3	19.1	21.5	17.88
		silage maize	10.96	12.28	11.96	18.14	11.86	12.24	13.35	9.9
		Winter wheat	17.84	14.60	18.23	17.45	17.21	15.43	14.73	16.34
	RMSE	Sugar beet	46.15	44.8	45.33	45.33	40.98	48.49	43.54	45.71

		Consumption potato	36.57	39.68	35.77	43.59	30.76	34.53	40.25	35.11
		silage maize	22.96	23.06	24.28	34.05	23.24	24.36	27.29	19.28
		Winter wheat	22.55	17.99	16.08	19.56	19.43	17.70	17.18	18.61
	PBIAS	Sugar beet	-1.86	-0.57	-2.5	1.33	-0.3	-3.2	-2.24	2.84
		Consumption potato	-3.33	-2.32	-5.47	-2.03	-3.17	-3.72	-3.25	-2.52
		silage maize	-0.96	0.75	0.25	0.85	-0.09	0.17	0.19	0.75
		Winter wheat	8.92	7.18	8.08	8.8	8.68	7.53	7.23	8.21

Table 13. Validation results of applying Cropmarkers algorithm on half canopy crop

phenological stage	Matrices	Models / Crop type	M5	M7	M51	M52	M53	M71	M72	M73
Emergence	MAE	Tulip	31.57	33.25	34.26	33.60	33.0	33.33	34.03	34.17
		Onion	14.78	15.40	12.07	18.41	15.44	11.29	13.5	14.84
	RMSE	Tulip	43.21	46.06	46.46	45.72	45.97	45.7	45.55	45.75
		Onion	27.28	27.26	24.44	27.91	25.2	24.35	27.02	23.0
	PBIAS	Tulip	4.16	2.77	5.64	3.42	1.73	8.2	5.81	4.59
		Onion	-4.11	-4.48	2.73	9.67	-6.06	1.19	3.39	-6.24
Closure	MAE	Tulip	16.78	18.63	18.6	19.24	18.6	17.99	18.45	18.54
		Onion	21.11	21.7	12.92	17.27	22.73	13.28	14.66	21.44
	RMSE	Tulip	41.26	44.93	44.06	43.9	44.32	42.87	43.4	44.57
		Onion	32.18	32.25	26.92	28.02	30.58	27.31	29.88	28.01
	PBIAS	Tulip	-10.79	-11.97	-10.44	-11.07	-12.14	-8.13	-10.42	-11.39
		Onion	-7.34	-7.85	-0.72	6.03	-9.51	-1.98	-0.11	-9.41
Transition	MAE	Tulip	22.77	26.58	26.45	24.3	24.45	25.42	25.2	27.6
		Onion	26.12	27.17	16.37	17.16	28.61	17.3	18.3	26.35
	RMSE	Tulip	41.59	46.00	45.74	43.81	44.24	43.78	44.05	46.19
		Onion	37.97	38.28	31.32	30.07	36.68	31.96	34.63	33.43
	PBIAS	Tulip	-14.19	-15.84	-15.54	-14.33	-15.07	-13.31	-14.57	-15.89
		Onion	-8.53	-9.23	-2.47	3.15	-10.94	-3.5	-1.85	-10.49
Harvest	MAE	Tulip	51.78	55.05	55.92	55.58	53.88	51.09	64.13	52.48
		Onion	26.19	26.79	26.44	30.63	24.44	27.18	33.04	23.3
	RMSE	Tulip	75.89	78.51	81.73	78.53	76.61	75.03	88.85	75.79
		Onion	54.52	53.96	54.01	58.81	49.25	54.26	62.44	45.38
	PBIAS	Tulip	-11.94	-9.62	-5.47	-12.18	-12.64	-5.96	3.33	-2.71
		Onion	1.13	1.62	2.14	3.48	0.87	2.98	7.42	0.76

7.3. Artificial Intelligence (AI) Statement

In the process of writing this thesis, ChatGPT is used to provide grammar and vocabulary checks for the written paragraphs, which aims to improve the quality of the text. Additionally, it offers some translation assistance when encountering difficulties during writing, such as unfamiliar words or complex sentence structures. All outputs from the AI are only used for assisting in writing and helping me improve my English writing. The content of the thesis is not influenced by the AI. A sample conversation link is provided below：

https://chat.openai.com/share/2e605ce2-71ee-4ec0-92b1-0d0be41f4a1b